ACS OMEGA

Article

http://pubs.acs.org/journal/acsodf

Microfibrillar Polysaccharide-Derived Biochars as Sodium Benzoate Adsorbents

Dagang Liu,*[,†] Yi Zhu,[†] Zehui Li,[‡] Muye Xiao,[†] Chenyu Jiang,[†] Muzi Chen,[†] and Yunuo Chen[†]

[†]Department of Chemistry, Collaborative Innovation Center of Atmospheric Environment and Equipment Technology, Nanjing University of Information Science and Technology, Nanjing 210044, China

[‡]Key Laboratory of Green Process and Engineering, Institute of Process Engineering, Chinese Academy of Sciences, Beijing 100190, China

Supporting Information

ABSTRACT: Microfibrillar biochars of chitin (CTF), chitosan (CSF), and cellulose (CLF) were fabricated via green homogenization and a pyrolysis process, and were subsequently explored as adsorbents for removing over-released sodium benzoate (SB) in aqueous systems. The structure, composition, morphology, and adsorption behavior of the as-fabricated biochars were characterized. Results suggest that all biochars, with a microscaled fibrillar structure and foam-like network morphology, underwent severe chemical transition during the pyrolysis process, thereby causing an enhancement of the Brunauer−Emmett−Teller surface area, pore volume, and aromatic and carbonaceous composition. Consequently, N-doped porous CTF/CSF microfibrillar biochars displayed a distinguished capture capacity toward SB compared to that of their fibrillar precursors. Tailoring the chemical composition, porous structure, and sorption mechanism constitutes a possible strategy to achieve adequate structural effects of polysaccharide microfibrillar chars for potential application in environmental treatment or bioenergy.

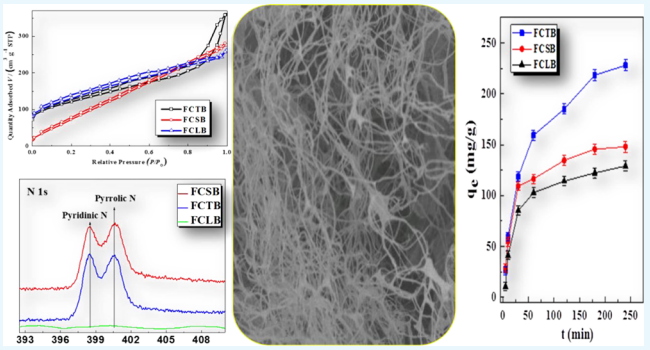

INTRODUCTION

Environmental pollution has become a great threat to both ecological environment and human health with rapid industrial development and population growth.[1,2] Organic matter continuously over-released from various chemical engineering industries and food and textile processes have caused serious environmental contamination in soil, water, and air, thus leading to potential threats to biological and human health even at very low concentrations.[3−5] Sodium benzoate (SB), used as a popular food preservative, inhibits microbial growth, and it is recommended by Joint Food and Agriculture Organization of the United Nations/World Health Organization expert committee on food additives that the acceptable daily intake (ADI) levels of SB should be 5 mg/kg body weight.[6,7] Consumption of SB beyond its ADI levels may be toxic and endangers the exposed population; it may even cause nausea, vomiting, diarrhea, rhinitis, bronchospasm, migraine, anaphylaxis, hyperactivity, and, at times, death, in extreme cases.[8−10] Recently, excessive SB released from food industries into water has gained significant environmental concern.

Various adsorbents, such as activated aluminum oxide, fly ash, zeolite, sand, and activated carbon, have been investigated and applied at actual sites for organic treatments,[11−15] especially biochar, a solid material having more hydrogen and oxygen components than those in activated carbon, is still in high demand as one of the effective low-cost sorbents.[16] Active biochar, fabricated by thermochemical conversion of biomass in an oxygen-limited environment,[17] has been widely explored for soil improvement, waste management, climate change mitigation, and energy production by alternating the bulk surface area, pore-size distribution, particle-size distribution, density, and packing.[18] More recently, biochars have been shown great benefit in the adsorption process of hydrocarbons, aromatic organics, and inorganic metal ions in aqueous systems due to their surface functional groups and highly efficient adsorption capacity.[19]

In our previous work, microfibrillar cellulose (CLF), chitin (CTF), and chitosan (CSF) were successfully prepared by a novel joint mechanical defibrillation process of homogenization and wet-grinding.[20−22] These three polysaccharide microfibrils or nanofibrils, with a diameter of 50 nm, have cross-linked porous networks and a high specific area and have been explored as highly efficient adsorbents in the form of biodegradable films or foams for aqueous heavy metal ions.[22−24] However, the lifespan of these naturally resourced polysaccharide nanofibrils as environmental adsorbents would be shortened due to easy biodegradation in wet surroundings. Aiming at addressing the issue of extending the lifespan of these microfibrils as pollutant adsorbents for industrial waste, we fabricated three microfibrillar

Received: April 5, 2017
Accepted: June 13, 2017
Published: June 27, 2017

DOI: 10.1021/acsomega.7b00404
ACS Omega 2017, 2, 2959−2966

polysaccharide biochars bearing functional groups via pyrolysis in this follow-up work. Subsequently, we investigated the effects of initial pH, temperature, adsorbent dosage, and initial concentration of the solution on the SB adsorption performance of the generated biochars.

RESULTS AND DISCUSSION

Biomass pyrolysis is a comprehensive process accounting for the physicochemical structure and properties of the solid feedstock and vapor products as well as the intermediate liquid. Typical thermogravimetry (TG) and derivative thermogravimetric (DTG) curves of polysaccharide microfibrils of CLF, CSF, and CTF are shown in Figure 1. The thermal degradation profiles of

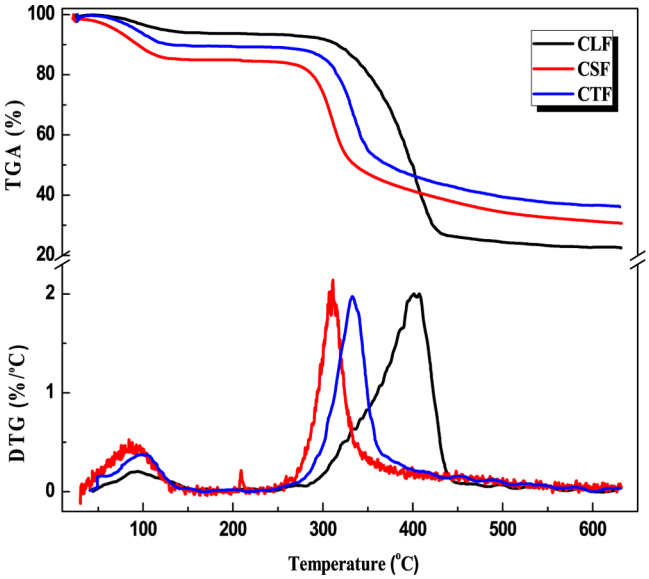

Figure 1. TG and DTG thermograms of CLF, CSF, and CTF.

CLF, CSF, and CTF displayed two sharp mass loss stages, corresponding to two major derivative peaks, that is, one peak occurring at around 100 °C for all three samples, ascribed to the evaporation of the water and/or bound water of the hydrophilic polysaccharide, and the other peak at around 270−450 °C, designated to maximum thermal degradation of CTF, CSF, and CLF. In accordance to the temperature at maximum rate of degradation (T_{max}), three polysaccharide microfibrils exhibited totally different individual thermal depletion performance, for example, the lowest T_{max} of thermal decomposition of CSF at around 310 °C was mainly aroused by the rupture of glucosamine and residues of acetyl glucose amine units in CSF chains.[25,26] The thermal degradation peak at around 335 °C for CTF was due to the depolymerization of CTF, with the formation of volatile low-molecular-weight products as well as char.[27,28] In the case of CLF, the maximum decomposition occurring at around 420 °C was attributed to the rupture of the xylan main chain and pyrolysis of CLF.[29,30] On the basis of the T_{max} of the three microfibrillar polysaccharides, their thermal stability follows the sequence CLF > CTF > CSF. It is known that the biochar yield is variable, depending on the pyrolysis condition and biomass feedstock. On the basis of the weight percent of charred residues, the biochar yield of FCTB, FCSB, and FCLB was estimated to be 22.41, 20.59, and 36.04%, respectively.

Carbonization processes of solid phases must involve phase changes in crystalline and amorphous polymers as well as breakage and formation of chemical bonds.[30] The elementary compositions of FCTB, FCSB, and FCLB, measured with an elemental analyzer, are listed in Table 1. All microfibrillar biochars exhibited a higher C content (70.24−78.19%) than that of their precursor (40.00−50.71%) but lower H (2.13−2.94%) and O (11.18−21.02%) contents than those of their precursor (6.43−7.70% of H and 42.06−44.89% of O) because a lot of common volatiles, like H_2O, CO_2, acetyl compounds, bio-oil constituents, pyrans, and high-weight anhydrosugars, were released during the charring process.[29] Corresponding to TG analysis, dehydration is the main process for weight loss in the chemical reaction between hydroxyl groups and/or in the repolymerization of pyrolysis products; CO_2 was mainly resourced from the depletion of ring-opened pyrolysis products. During the charring process of CTF and CSF, acetyl compounds were thought to be one of the volatiles that were released from the cleavage of the side-chain amide. Consequently, the release of these volatiles leads to a greater loss of O, which decreased from 42.06−44.89 to 11.18−21.02% in content. After pyrolysis, H/C and O/C atomic ratios decreased sharply, implying that these biochars became increasingly more aromatic and carbonaceous. Besides, the H/C rate of only 3% of all biochars indicates that much amorphous surface carbon was produced during the charring process of amorphous carbon (also evidenced by X-ray diffraction (XRD) in Figure S1 in Supporting Information). Therefore, the charring pyrolysis has a significant impact on the elementary ratio, chemical structure, and composition of the biomass char. To further ascertain the elemental form in biochars, the general X-ray photoelectron spectroscopy (XPS) spectra and respective XPS spectra of the core levels, C 1s, N 1s, and O 1s, are presented in Figure 2. According to the binding energy values and the corresponding assessments of FCTB, FCSB, and FCLB, C 1s could be fitted into two components (Figure 2b). The component at 284.5 eV is commonly assigned to aliphatic carbon (C−C/C−H), whereas the other one centered at 286.1 eV is assigned to the C−N group and the carbon connected with hydroxyl (C−OH) and/or O−R groups (C−OR). Accordingly, O 1s spectra of FCLB (Figure 2c) show

Table 1. Parameters of Brunauer−Emmett−Teller (BET) Surface Area (S_{BET}), Pore Volume, Elementary Composition (%), and Atomic Ratios of FCTB, FCSB, FCLB, and Their Microfibril Precursors

	elementary composition			atomic ratios						
fibrils	N	C	H	H/C	O/C	C/N	S_{BET}[a] (m^2/g)	V_t[b] (cm^3/g)	V_{mic}[c] (cm^3/g)	V_{mic} (%)
FCTB	6.61	70.24	2.13	0.03	0.30	10.63	422.87	0.56	0.16	29.48
FCSB	10.31	75.87	2.64	0.03	0.15	7.36	357.41	0.43	0.07	15.46
FCLB	0	78.19	2.94	0.03	0.24		459.73	0.41	0.17	41.86
CTF	6.62	44.89	6.43	0.14	0.94	6.78				
CSF	7.41	40.00	7.70	0.19	1.12	5.40				
CLF	0	50.71	7.12	0.14	0.83					

DOI: 10.1021/acsomega.7b00404
ACS Omega 2017, 2, 2959−2966

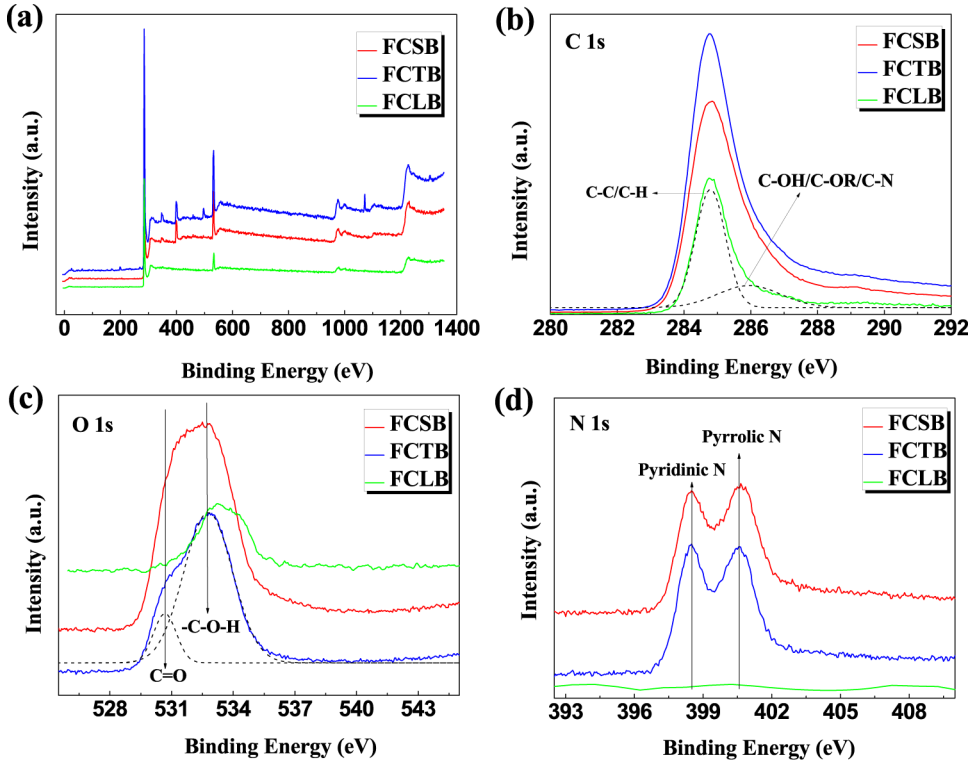

Figure 2. General XPS spectra (a) and individual XPS spectra of C 1s (b), O 1s (c), and N 1s (d) for FCTB, FCSB, and FCLB, respectively.

only one peak at 532.7 eV (−C−OH), and the O 1s peaks for both FCTB and FCSB, located at 531.2 eV (shoulder peak) and 532.7 eV (main peak), are attributed to −C═O and −C−OH, respectively, implying the presence of some carboxylic and hydroxyl groups in the char. With the absence of N in FCLB, a high resolution of N 1s for both FCTB and FCSB displayed double individual peaks, attributed to the pyridinic-N centered at 398.5 eV and the pyrrolic-N centered at 400.5 eV,[31] respectively (Figure 2d), indicating that the $-NH_2$ side group was partly converted into aromatic pyridinic-N and pyrrolic-N,[32] thus leading to much of the amorphous aromatic carbon (also evidenced by XRD in Figure S1) transforming during the charring process.

The morphologies of the three microfibrillar biochars are shown in Figure 3. FCTB microfibrils inherited the morphology of a random crosslinking network of CTF isolated from biological chitin lamellar layer (Figure 3a,b). CTF biochars were composed of microfibrils with average widths of 200 ± 10 nm, much larger than the diameter of the CTF precursor (50 nm).[22] Porous FCSB, as shown in Figure 3c,d, displayed less uniform (100−500 nm) and thicker microfibrils and a denser network than those of FCTB, indicating a compact stack through $\pi-\pi$ or electrostatic interactions. However, FCLB is considered to have plenty of mutually bundled and layered microfibrils with severe aggregation into laminar microstructures (Figure 3e,f).[33] Above all, the CLF/CTF/CSF biochars exhibit a much larger microfibrillar diameter than that of their precursor, which was presumably ascribed to the burn-off of the completely isolated tiny fibrils being charred at 600 °C, thereby causing an increment of pore volume. As listed in Table 1, the S_{BET} values of FCLB, FCTB, and FCSB were 459.73, 422.87, and 357.41 m^2/g, respectively, which are highly related to their microporosities ($V_{mic}{}^c$) of 41.86, 29.48, and 15.46%, respectively. It is worth noting that the pore space of FCTB is the highest but the microporous space and specific surface areas of FCLB are the highest among those of the three biochars. Biochars generated from charged CSF microfibrils preferably formed a mesoporous or macroporous network, which was revealed by their relatively high total pore volume but very low microporous volume.

Besides the structure and morphology of the biochar, many parameters strongly influenced the adsorption behavior when the biochar was used to capture aqueous SB. Figure 4a illustrates the pH dependence of the adsorption of SB. All biochars exhibited similar pH-dependent adsorption behaviors, that is, the adsorption capacity of the SB electrolyte increased with an increase in the pH from 3 to 7 and subsequently reduced as the pH increased from 7 to 9. Maximum adsorption capacity values of 385.46, 335.23, and 261.87 mg/g were achieved at a solution pH of about 7, corresponding to FCSB, FCTB, and FCLB, respectively, indicating higher adsorption amounts at a low ionic concentration (neutral pH) than those at high ionic concentration (acidic or alkaline condition). Besides, it is worth noting that the adsorption capacity of FCSB was higher than that of FCTB in acidic solutions (pH 4−7) but the opposite trend was seen at pH 7.75−9.00, which indicates that the adsorption process was dramatically affected by the ionic interaction between the adsorbent and adsorbate.[34] The temperature dependence of removal amount of SB at pH 6.58 is shown in Figure 4b. The removal amount of SB decreases from 206.14, 311.54, and 154.06 to 68.96, 41.37, and 34.48 mg/g for FCTB, FCSB, and FCLB, respectively, as the adsorption temperature rises from 10 to 60 °C, thus confirming an exothermic capture process in nature. The negative temperature effect of biochars was probably because of the temperature dependence on ionization and chemical potential of SB and the adsorbents. Figure 5a shows the dependence of the initial concentration of SB on the adsorption capacity of FCTB, FCSB, and FCLB. At a fixed adsorbent dose, the adsorption amount of SB increased as

DOI: 10.1021/acsomega.7b00404
ACS Omega 2017, 2, 2959−2966

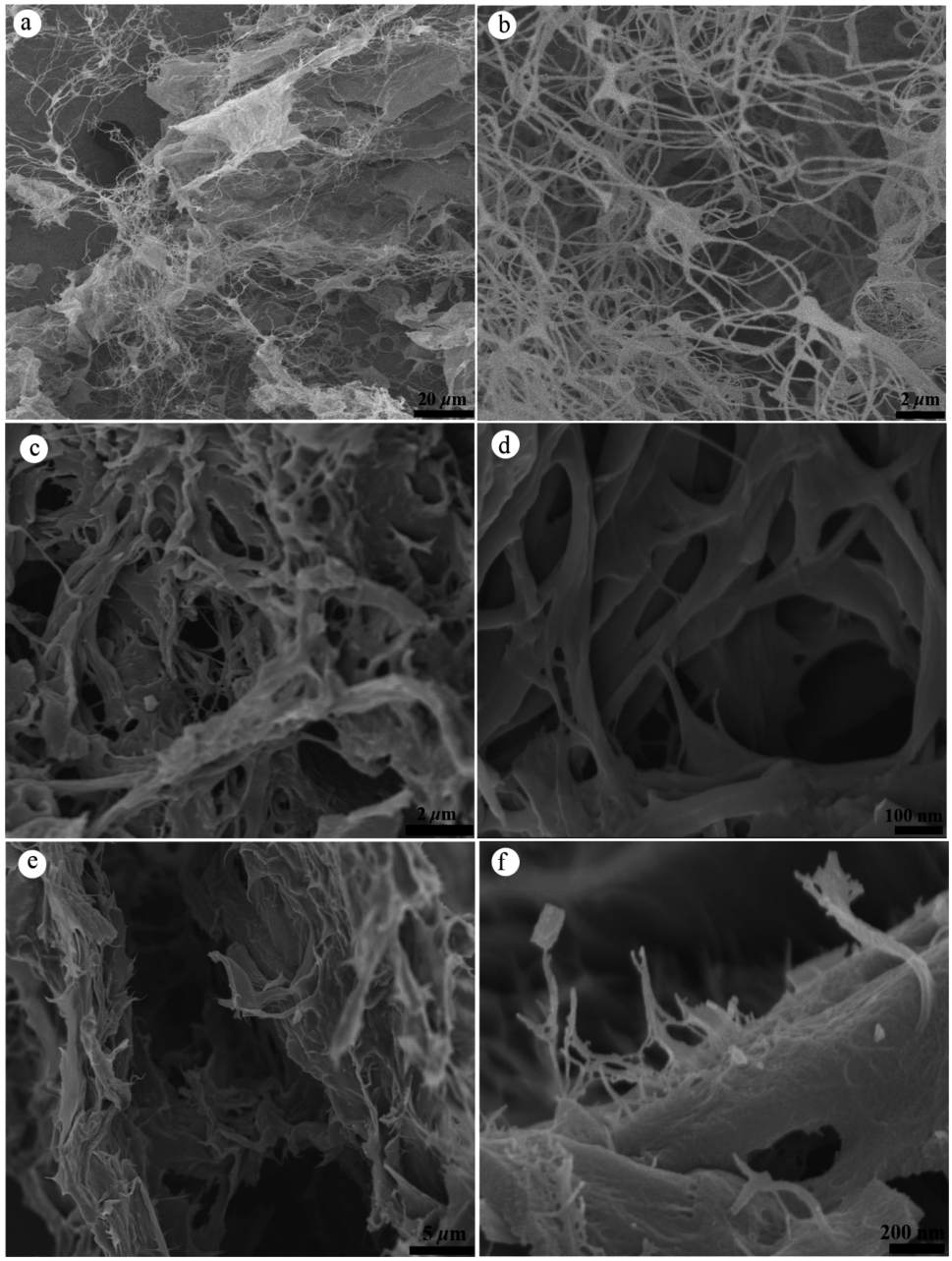

Figure 3. Field emission-scanning electron microscopy (FE-SEM) micrographs of FCTB (a, b), FCSB (c, d), and FCLB (e, f).

the concentration of SB increased. The experimental equilibrium adsorption amounts (q_{exp}) of SB, as listed in Table 2, are 227.96, 148.01, and 129.02 mg/g for FCSB, FCTB, and FCLB, respectively, indicating that the adsorption sites actively accommodated SB at high concentrations. In comparison to their precursors, CSF, CTF, and CLF, the three biochars exhibit a 2- to 4-fold increase in q_{exp} because of their high specific surface area, which was readily accessible to accommodate much more SB. Among the three chars, FCSB show the highest adsorption capacity toward SB, which is mainly attributed to its aromatic π-system and functional pyridinic-N and pyrrolic-N groups, thus promoting $\pi-\pi$ affinity and ionic interactions between them. Especially in acid solution, more protons were available to hydrolyze and protonate into quaternary ammonium and compete with SB to occupy the adsorption sites. Therefore, it can be concluded that the high BET surface area, pore volume, and functional groups of the microfibrillar biochar played important roles in the sorption behavior.

In general, the isothermal adsorption process was illustrated by the Langmuir and Freundlich models.[35,36] The nonlinear form of the Langmuir isotherm is presented as eq 1.

$$q_e = \frac{q_m\left(\frac{1-R_L}{R_L C_0}\right)C_e}{1+\left(\frac{1-R_L}{R_L C_0}\right)C_e} \quad (1)$$

where C_0 and C_e are the initial and equilibrium concentrations of the adsorbate (mg/L), respectively; q_e is the amount of adsorbate adsorbed per unit mass of adsorbent (mg/g); and q_m is the theoretical maximum adsorption capacity (mg/g). R_L is a parameter indicating whether the adsorption is irreversible (R_L

DOI: 10.1021/acsomega.7b00404
ACS Omega 2017, 2, 2959−2966

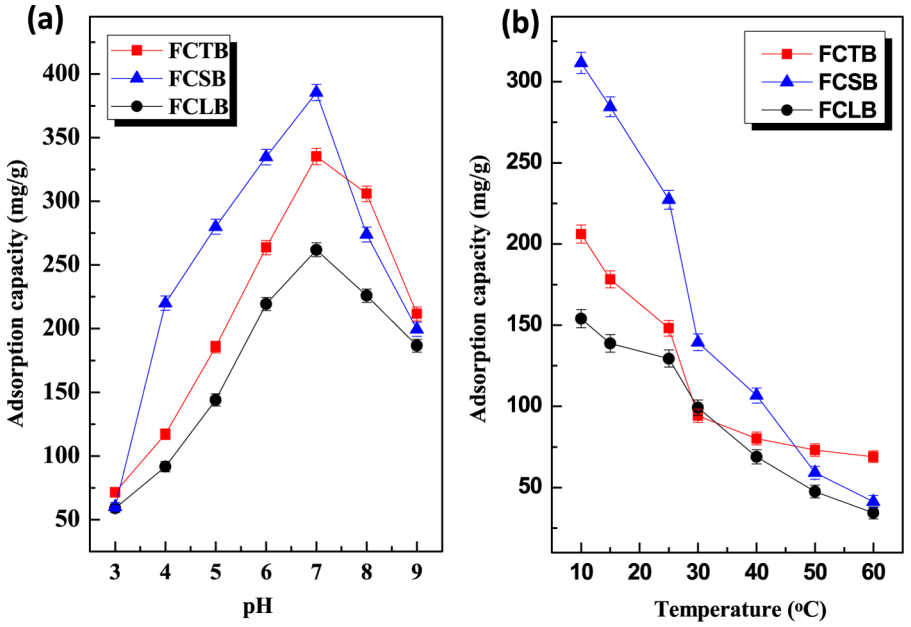

Figure 4. (a) Effects of pH value on the adsorption capacity of SB onto FCTB, FCSB, and FCLB and (b) temperature dependence on the adsorption capacity of SB onto FCTB, FCSB, and FCLB.

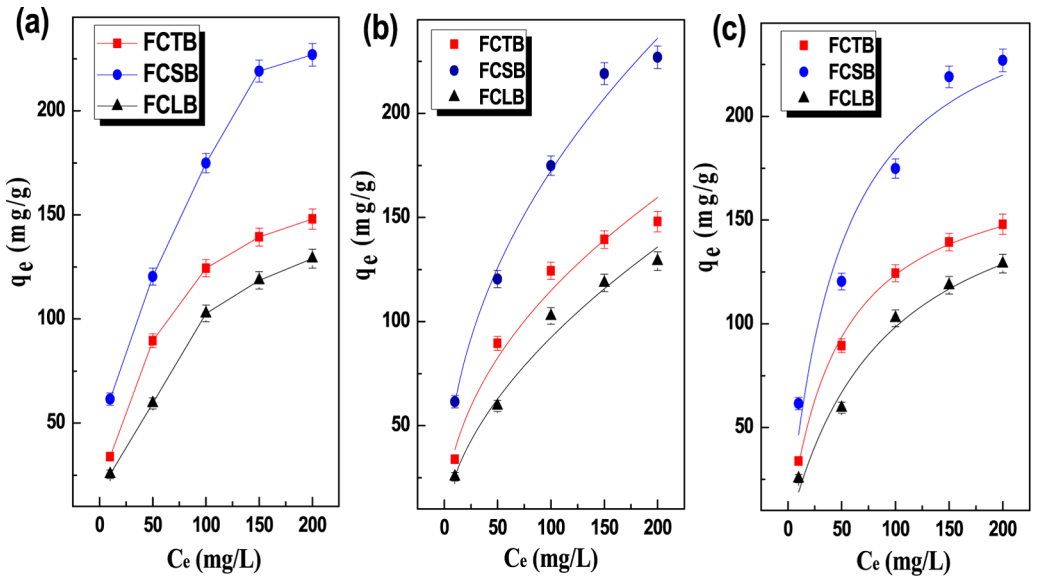

Figure 5. Effects of initial SB concentration on the adsorption capacity (a); Freundlich (b) and Langmuir (c) isothermal adsorption models for the adsorption of SB onto FCTB, FCSB, and FCLB, respectively (240 min, 298.15 K, pH = 6.86).

= 0), favorable ($0 < R_L < 1$), linear ($R_L = 1$), or unfavorable ($R_L > 1$).

The Freundlich isotherm is described as eq 2

$$q_e = K_F C_e^{1/n} \quad (2)$$

where K_F is the Freundlich isotherm constant indicating the adsorption capacity and n is the adsorption intensity. The fitting plots based on the Langmuir and Freundlich models for the adsorption isotherm are shown in Figure 5b,c, and the calculated values of the related parameters are listed in Table 2. In the Langmuir isotherm, the R_L values are in the range of $0 < R_L < 1$, which indicates that the adsorbent surface has sites of identical energy, allowing the formation of adsorbate monolayers. Parameter, n, in the Freundlich isotherm is related to the degree of surface heterogeneity.[37] When the $1/n$ value is close to 1 or even 1, the adsorption at the binding sites is thought to be nearly homogeneous. The $1/n$ values of FCTB, FCSB, and FCLB were 0.4184, 0.4098, and 0.5128, respectively. Judging by the R^2 of the two models, the adsorption of SB onto FCTB, FCLB fit the Langmuir better than it fit the Freundlich isotherm, suggesting a monolayer chemical sorption. However, the Freundlich isotherm provides a better fit for FCSB, depicting a multilayer adsorption process dominated by ionic interaction.

Figure 6 shows the time dependence of the adsorption capacity of the biochars (a) and their (b) pseudo-first- and (c) pseudo-second-order adsorption kinetic models. All micro-fibrillar biochars exhibit a fast and efficient uptake of SB in the initial few minutes (0−10 min) and achieve subsequent equilibrium within 4 h. Two kinetic models, that is, the pseudo-first- and pseudo-second-order models, were fitted to

DOI: 10.1021/acsomega.7b00404
ACS Omega 2017, 2, 2959−2966

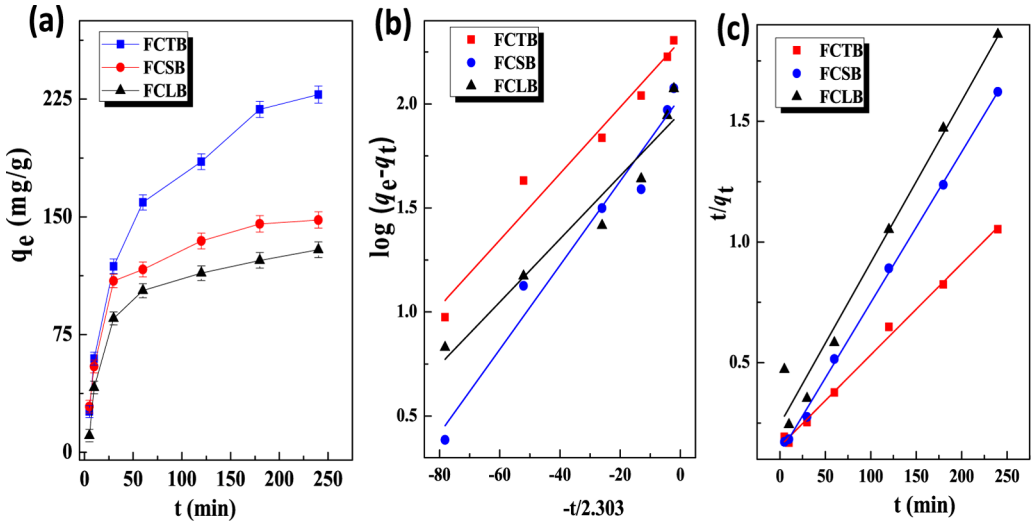

Figure 6. Contact time dependence on the adsorption capacity (a) and plots of the (b) pseudo-first-order and (c) pseudo-second-order adsorption kinetic models for the adsorption of SB onto FCTB, FCSB, and FCLB, respectively (298.15 K, pH = 6.86).

Table 2. Langmuir and Freundlich Isotherm Parameters and Kinetic Parameters for the Adsorption of SB onto FCTB, FCSB, and FCLB (240 min, 298.15 K, pH = 6.86)

		Langmuir			Freundlich			pseudo-first-order model			pseudo-second-order model		
	q_{exp} (mg/g)	q_m (mg/g)	R_L	R^2	$1/n$	K_F (mg/g)	R^2	k_1 (min^{-1})	q_e (mg/g)	R_1^2	k_2 (g/mg min)	q_e (mg/g)	R_2^2
FCSB	227.96	288.25	0.21−0.84	0.9273	0.41	27.28	0.9810	0.024	200.91	0.9591	0.0001	264.55	0.9949
FCTB	148.01	180.37	0.17−0.81	0.9949	0.42	12.97	0.9652	0.046	107.89	0.9560	0.0002	166.67	0.9985
FCLB	129.02	188.35	0.30−0.89	0.9766	0.51	7.76	0.9713	0.036	90.57	0.9278	0.0002	149.48	0.9706
CSF	52.68												
CTF	50.06												
CLF	46.54												

provide an estimation of adsorption rates and potential reaction mechanism, which are described as follows, respectively

$$\log(q_e - q_t) = -\frac{K_1}{2.303}t + \log q_e \quad (3)$$

$$\frac{t}{q_t} = \frac{1}{q_e}t + \frac{1}{K_2 q_e^2} \quad (4)$$

where K_1 is the pseudo-first-order rate constant (min^{-1}), K_2 is the pseudo-second-order rate constant (min^{-1}), and q_e and q_t are the amounts of SB adsorbed at equilibrium (mg/g) and at time t (mg/g), respectively. The kinetic parameters (q_e, K_1, K_2), correlation coefficients (R_1^2, R_2^2), and adsorption capacity of the microfibrillar biochars were calculated and are listed in Table 2. In comparison with the R_1^2 values of the three biochars, the R_2^2 values of FCSB, FCTB, and FCLB were 0.9949, 0.9985, and 0.9706, respectively. Obviously, a better fit of the pseudo-second-order kinetics model for all biochars indicates that a diffusion mechanism and chemical interaction were involved in the sorption process.

CONCLUSIONS

A green process of homogenization and pyrolysis was deployed to prepare pure microfibrillar biochars sourced from the polysaccharides CLF, CTF, and CSF. Compared with their fibrillar precursors, the biochars consisted of relatively thick fibrils, large specific surface areas, and loose porous networks because the tiny fibrils were burnt-off during the pyrolysis process. Meanwhile, the amount of hydroxyl groups might be reduced for all microfibrils, whereas the functional groups of pyridinic-N and pyrrolic-N were transformed in FCTB and FCSB. These biochars captured varied isothermal equilibrium amounts of SB at about 227.96, 148.01, and 129.02 mg/g corresponding to FCSB, FCTB, and FCLB, respectively. We built sorption models of kinetics and dynamics and discovered that the sorption of SB onto microfibrillar biochars involves diffusion and chemical sorption; specifically, the sorption was monolayer chemical sorption on the homogenous surfaces of FCTB and FCLB, whereas the multilayer process was preferred for FCSB.

EXPERIMENTAL SECTION

Raw chitin and chitosan powders, with deacetylation degrees of 6 and 90% and molecular weights (M_w) of 203.19 and 161.16 kDa, respectively, were obtained from Jiachen Chemical Company (Shanghai, China). Microcrystalline cellulose (MCC, bulk density 0.6 g/mL at 25 °C) of analytical grade was purchased from Sinopharm Chemical Reagent Co., Ltd. (Shanghai, China). SB of analytical grade was purchased from Bodi Chemical Co., Ltd. (Tianjin, China).

As described in our previous work,[20−22] a certain amount of raw chitin powder (5 mg) was poured into distilled water (1 L) and stirred overnight to obtain a slurry at room temperature. Then, the slurry was poured into a cylindrical wet-grinding machine (LABOR-PILOT 2000/4; IKA-Works, Inc.) and continuously shear-flowed through a milling gap of about 0.2 mm for 20 cycles at a flow speed of 10 L/h. Subsequently, the

DOI: 10.1021/acsomega.7b00404
ACS Omega 2017, 2, 2959−2966

milling-dispersed chitin suspension was pumped through a high-pressure homogenizer (M-100P; Microfluidics) under a constant pressure of 250 MPa for 10 cycles. The as-prepared viscose dispersion was then freeze-dried into fibrillar foams, which were labeled as CTF microfibril. Using the same method of mechanical defibrillation described above, CSF and CLF microfibrils were also prepared and freeze-dried into foams. Furthermore, the as-fabricated microfibrillar polysaccharide foams were packaged in foil and subsequently subjected to pyrolysis at 600 °C for 1 h under nitrogen atmosphere. Ultimately, the biochars produced by pyrolysis from feedstock biomasses of CTF, CSF, and CLF were labeled as FCTB, FCSB, and FCLB, respectively.

The parameters, such as pH, adsorbent dose, initial concentration of adsorbates, contact time, and temperature, that influenced the adsorption behaviors of the biochars were investigated. Briefly, a fixed amount of biochar (5 mg), used in batch adsorption tests, was poured into an aqueous solution of SB in an orbital shaker at 180 rpm. By varying the pH of the adsorption solution from 3 to 9, the temperature from 10 to 60 °C, the initial concentration of SB from 0 to 200 mg/L, and the sorption time from 0 to 250 min, adsorption equilibrium was achieved. After equilibrium adsorption, the samples were filtered using 0.45 μm nylon syringe filters prior to analysis on a UV spectrophotometer at 223.5 nm. The adsorption capacity (q, mg/g) and adsorption isotherms of SB were then obtained by mass-balance calculations according to the following equation

$$q_e = \frac{(C_0 - C_e)V}{m} \quad (5)$$

where C_0 and C_e are the initial and equilibrium concentrations of SB (mg/L), respectively, V is the volume of the adsorbate solution (L), and m is the weight of the adsorbent (g). The effect of the initial pH, measured by a pH meter (PHS-25B; Jintan, China), on the adsorption of SB by biochar was evaluated by adjusting the solution pH with a 0.1 M solution of HCl or NaOH.

The specific surface area was analyzed by the BET nitrogen adsorption−desorption method using a Micromeritics ASAP 2020 HD88 analyzer. The biochars FCTB, FCSB, and FCLB were vacuum-degassed overnight at 100 °C. The BET surface area was then measured and calculated under a relative pressure range (P/P_0) of 0.05−0.3 and a N_2 gas atmosphere. Thermal degradation tests of the CLF, CSF, and CTF samples were carried out on a TG analyzer (TG/DSC1; Mettler Toledo, Switzerland) in a dry nitrogen atmosphere. The samples were heated from 20 to 600 °C at a rate of 10 °C/min and then held for 30 min at 600 °C prior to cooling at a rate of 20 °C/min. Weight loss percentage versus temperature and derivate weight loss against temperature were plotted for thermogravimetric and DTG analyses. Elemental analysis (C, H, N, and O) of the microfibrils and microfibrillar biochars was conducted on with an elemental analyzer (vario EL III; Elementar Analysensysteme GmbH, Germany). Morphological observations of FCTB, FCSB, and FCLB were carried out on an FE-SEM (JSM-6700F; Hitachi, Japan) at 20 kV voltage. The samples were coated with gold prior to FE-SEM visualization. Surface chemical compositions of FCTB, FCSB, and FCLB were measured using an XPS spectroscope (ESCALAB 250Xi; Thermo Fisher Scientific) with a monochromic Al Kα source ($h\nu$ = 1486.7 eV) at a voltage of 15 kV and an emission current of 10 mA. Survey spectra were an average of eight scans at a pass energy of 200 eV, an energy step size of 1 eV, and a dwell time of 100 ms. The concentration of the SB solutions was determined using a UV−vis spectrophotometer (UV-3600; Shimadzu Corp., Japan) at a maximum absorbance wavelength of 223.5 nm.

■ ASSOCIATED CONTENT

Supporting Information

The Supporting Information is available free of charge on the ACS Publications website at DOI: 10.1021/acsomega.7b00404.

XRD patterns of FCTB, FCSB, and FCLB; FTIR spectra of the biochars with or without captured SB (PDF)

■ AUTHOR INFORMATION

Corresponding Author

*E-mail: dagangliu@gmail.com, dagang@nuist.edu.cn.

ORCID

Dagang Liu: 0000-0002-1320-7030

Notes

The authors declare no competing financial interest.

■ ACKNOWLEDGMENTS

The authors are grateful to the National Natural Science Foundation of China (Nos. 51473077 and 21277073), CSC scholarship (201608320064), and Six Talented Peak Program, 333 High-Level Talent Cultivation Program of Jiangsu Province and Program of Jiangsu Province to Encourage Graduate Students to Innovate for financial support. The Support Program of the Priority Academic Program Development of Jiangsu Higher Education Institutions is also acknowledged.

■ REFERENCES

(1) McMichael, A. J. Globalization, climate change, and human health. *N. Engl. J. Med.* **2013**, *368*, 1335−1343.

(2) Valipour, M.; Mousavi, S. M.; Valipour, R. Air, water, and soil pollution study in industrial units using environmental flow diagram. *J. Basic Appl. Sci. Res.* **2012**, *2*, 12365−12372.

(3) Phillips, D. J.; Gibson, M. I. Redox-sensitive materials for drug delivery: targeting the correct intracellular environment, tuning release rates, and appropriate predictive systems. *Antioxid. Redox Signaling* **2014**, *21*, 786−803.

(4) Ahmad, M.; Soo, L. S.; Yang, J. E.; et al. Effects of soil dilution and amendments (mussel shell, cow bone, and biochar) on Pb availability and phytotoxicity in military shooting range soil. *Ecotoxicol. Environ. Saf.* **2012**, *79*, 225−231.

(5) Mohan, D.; Pittman, Jr. Arsenic removal from water/wastewater using adsorbents-A critical review. *J. Hazard. Mater.* **2007**, *142*, 1−53.

(6) Lennerz, B. S.; Vafai, S. B.; Delaney, N. F.; et al. Effects of sodium benzoate, a widely used food preservative, on glucose homeostasis and metabolic profiles in humans. *Mol. Genet. Metab.* **2015**, *114*, 73−79.

(7) Das, M.; Dixit, S.; Mishra, K. K.; Khanna, S. K. Benzoate and synthetic color risk assessment for fast food sauces served at street food joints of Lucknow India. *Am. J. Food Technol.* **2008**, *3*, 183−191.

(8) Fujitani, T. Short-term effect of sodium benzoate in F344 rats and B6C3F1 mice. *Toxicol. Lett.* **1993**, *69*, 171−179.

(9) Brahmachari, S.; Pahan, K. Sodium benzoate, a food additive and a metabolite of cinnamon, modifies T cells at multiple steps and inhibits adoptive transfer of experimental allergic encephalomyelitis. *J. Immunol.* **2007**, *179*, 275−283.

(10) Pongsavee, M. Effect of sodium benzoate preservative on micronucleus induction, chromosome break, and ala40thr superoxide dismutase gene mutation in lymphocytes. *BioMed. Res. Int.* **2015**, *2015*, No. 103512.

(11) Hale, S. E.; Lehmann, J.; Rutherford, D.; Zimmerman, A. R.; Bachmann, R. T.; Shitumbanuma, V.; OToole, A.; Sundqvist, K. L.; Arp, H. P. H.; Cornelissen, G. Quantifying the total and bioavailable polycyclic aromatic hydrocarbons and dioxins in biochars. *Environ. Sci. Technol.* **2012**, *46*, 2830−838.

DOI: 10.1021/acsomega.7b00404
ACS Omega 2017, 2, 2959−2966

(12) Muzzarelli, R. A. A.; Boudrant, J.; Meyer, D.; et al. A tribute to Henri Braconnot, precursor of the carbohydrate polymers science, on the chitin bicentennial. *Carbohydr. Polym.* **2012**, *87*, 995−1012.
(13) Wang, S.; Sun, H.; Ang, H. M.; Tadé, M. O. Adsorptive remediation of environmental pollutants using novel graphene-based nanomaterials. *Chem. Eng. J.* **2013**, *226*, 336−347.
(14) Kushwaha, J. P.; Srivastava, V. C.; Mall, I. D. Treatment of dairy wastewater by commercial activated carbon and bagasse fly ash: parametric, kinetic and equilibrium modelling, disposal studies. *Bioresour. Technol.* **2010**, *101*, 3474−3483.
(15) Popuri, S. R.; Vijaya, Y.; Boddu, V. M.; Abburi, K. Adsorptive removal of copper and nickel ions from water using chitosan coated PVC beads. *Bioresour. Technol.* **2009**, *100*, 194−199.
(16) Mohan, D.; Sarswat, A.; Ok, Y. S.; Pittman, C. U. Organic and inorganic contaminants removal from water with biochar, a renewable, low cost and sustainable adsorbent-a critical review. *Bioresour. Technol.* **2014**, *160*, 191−202.
(17) Ahmad, M.; Rajapaksha, A. U.; Lim, J. E.; Zhang, M.; Bolan, N.; Mohan, D.; Vithanage, M.; Lee, S. S.; Ok, Y. S. Biochar as a sorbent for contaminant management in soil and water: a review. *Chemosphere* **2014**, *99*, 19−33.
(18) Beesley, L.; Moreno-Jiménez, E.; Gomez-Eyles, J. L.; Harrisd, E.; Robinsond, B.; Sizmure, T. A review of biochars' potential role in the remediation, revegetation and restoration of contaminated soils. *Environ. Pollut.* **2011**, *159*, 3269−3282.
(19) Chen, B.; Zhou, D.; Zhu, L. Transitional adsorption and partition of nonpolar and polar aromatic contaminants by biochars of pine needles with different pyrolytic temperatures. *Environ. Sci. Technol.* **2008**, *42*, 5137−5143.
(20) Liu, D.; Wu, Q.; Chang, P.; Chen, M. Chitosan colloidal suspension composed of mechanically-disassembled nanofibers. *J. Colloid Interface Sci.* **2011**, *354*, 637−643.
(21) Liu, D.; Ma, Z.; Wang, Z.; Tian, H.; Gu, M. Biodegradable poly (vinyl alcohol) foams supported by cellulose nanofibrils: processing, structure and properties. *Langmuir* **2014**, *30*, 9544−9550.
(22) Liu, D.; Zhu, Y.; Li, Z.; et al. Chitin nanofibrils for rapid and efficient removal of metal ions from water system. *Carbohydr. Polym.* **2013**, *98*, 483−489.
(23) Liu, D.; Li, Z.; Zhu, Y.; et al. Recycled chitosan nanofibril as an effective Cu (II), Pb (II) and Cd (II) ionic chelating agent: adsorption and desorption performance. *Carbohydr. Polym.* **2014**, *111*, 469−476.
(24) Ma, Z.; Liu, D.; Zhu, Y.; Li, Z.; Li, Z.; Tian, H.; Liu, H. Graphene oxide/chitin nanofibril composite foams as column adsorbents for aqueous pollutants. *Carbohydr. Polym.* **2016**, *144*, 230−237.
(25) Alonso, J.; Peniche-Covas, C.; Nieto, J. Determination of the degree of acetylation of chitin and chitosan by thermal analysis. *J. Therm. Anal.* **1983**, *28*, 189−193.
(26) Guo, Z.; Guo, A.; Guo, Q.; et al. Decomposition of dexamethasone by gamma irradiation: Kinetics, degradation mechanisms and impact on algae growth. *Chem. Eng. J.* **2017**, *307*, 722−728.
(27) Zhang, Q.; Chang, J.; Wang, T.; Xu, Y. Review of biomass pyrolysis oil properties and upgrading research. *Energy Convers. Manage.* **2007**, *48*, 87−92.
(28) Yang, H.; Yan, R.; Chen, H.; Lee, D. H.; Zheng, C. Characteristics of hemicellulose, cellulose and lignin pyrolysis. *Fuel* **2007**, *86*, 1781−1788.
(29) Wang, S.; Ru, B.; Lin, H.; Luo, Z. Degradation mechanism of monosaccharides and xylan under pyrolytic conditions with theoretic modeling on the energy profiles. *Bioresour. Technol.* **2013**, *143*, 378−383.
(30) Hale, S. E.; Lehmann, J.; Rutherford, D.; Zimmerman, A. R.; Bachmann, R. T.; Shitumbanuma, V.; OToole, A.; Sundqvist, K. L.; Arp, H. P. H.; Cornelissen, G. Quantifying the total and bioavailable polycyclic aromatic hydrocarbons and dioxins in biochars. *Environ. Sci. Technol.* **2012**, *46*, 2830−838.
(31) Yuan, H.; Deng, L.; Cai, X.; Zhou, S.; Chen, Y.; Yuan, Y. Nitrogen-doped carbon sheets derived from chitin as non-metal bifunctional electrocatalysts for oxygen reduction and evolution. *RSC Adv.* **2015**, *5*, 56121−56129.
(32) Zhang, L.; Wang, Y.; Peng, B.; Yu, W.; Wang, H.; Wang, T.; Deng, B.; Chai, L.; Zhang, K.; Wang, J. Preparation of a macroscopic, robust carbon-fiber monolith from filamentous fungi and its application in Li−S batteries. *Green Chem.* **2014**, *16*, 3926−3934.
(33) Nogi, M.; Kurosaki, F.; Yano, H.; Takano, M. Preparation of nanofibrillar carbon from chitin nanofibers. *Carbohydr. Polym.* **2010**, *81*, 919−924.
(34) Chai, K.; Ji, H. Dual functional adsorption of benzoic acid from wastewater by biological-based chitosan grafted β-cyclodextrin. *Chem. Eng. J.* **2012**, *203*, 309−318.
(35) Jeppu, G. P.; Clement, T. P. A modified Langmuir-Freundlich isotherm model for simulating pH-dependent adsorption effects. *J. Contam. Hydrol.* **2012**, *129−130*, 46−53.
(36) Langmuir, I. The constitution and fundamental properties of solids and liquids. *J. Am. Chem. Soc.* **1916**, *38*, 2221−2295.
(37) Site, A. D. Factors affecting sorption of organic compounds in natural sorbent/water systems and sorption coefficients for selected pollutants, a review. *J. Phys. Chem. Ref. Data* **2001**, *30*, 187−439.

DOI: 10.1021/acsomega.7b00404
ACS Omega 2017, 2, 2959−2966